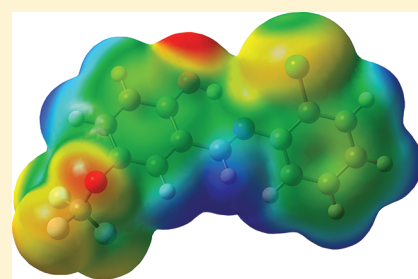


# Crystal Structure, Spectroscopy, and Quantum Chemical Studies of (*E*)-2-[(2-Chlorophenyl)iminomethyl]-4-trifluoromethoxyphenol

Hasan Tanak\*

Department of Physics, Faculty of Arts and Sciences, Amasya University, 05100 Amasya, Turkey

**ABSTRACT:** The Schiff base compound (*E*)-2-[(2-chlorophenyl)iminomethyl]-4-trifluoromethoxyphenol has been synthesized and characterized by IR, UV–vis, and X-ray single-crystal determination. The molecular geometry from X-ray experiment in the ground state has been compared using the density functional theory (DFT) with the 6-311++G(d,p) basis set. The calculated results show that the DFT can well reproduce the structure of the title compound. Using the TD-DFT method, electronic absorption spectra of the title compound have been predicted, and a good agreement is determined with the experimental ones. To investigate the tautomeric stability, optimization calculations at the B3LYP/6-311++G(d,p) level were performed for the enol and keto forms of the title compound. Calculated results reveal that its enol form is more stable than its keto form. The predicted



nonlinear optical properties of the title compound are much greater than those of urea. The changes of thermodynamic properties for the formation of the title compound with the temperature ranging from 200 to 500 K have been obtained using the statistical thermodynamic method. At 298.15 K, the change of Gibbs free energy for the formation reaction of the title compound is  $-824.841$  kJ/mol. The title compound can spontaneously be produced from the isolated monomers at room temperature. The tautomeric equilibrium constant is also computed as  $3.85 \times 10^{-4}$  at 298.15 K for enol $\leftrightarrow$ keto tautomerization of the title compound. In addition, a molecular electrostatic potential map of the title compound was performed using the B3LYP/6-311++G(d,p) method.

## 1. INTRODUCTION

Azomethines (known as Schiff bases), having imine groups (C=N) and benzene rings in the main chain alternately, and being  $\pi$ -conjugated, peak interest as materials for a wide spectrum of applications, particularly as corrosion inhibitors,<sup>1</sup> catalyst carriers,<sup>2,3</sup> thermo-stable materials,<sup>4–6</sup> metal ion complexing agents,<sup>7</sup> and in biological systems.<sup>8–10</sup> Schiff base compounds display interesting photochromic and thermochromic features in the solid state and can be classified in terms of these properties.<sup>11</sup> Photo- and thermochromism arise via H-atom transfer from the hydroxy O atom to the imine N atom.<sup>12,13</sup> Such proton-exchanging materials can be utilized for the design of various molecular electronic devices.<sup>14–16</sup> In general, *o*-hydroxy Schiff bases display two possible tautomeric forms, the enol-imine (OH) and the keto-amine (NH) forms (see Figure 1). Depending on the tautomers, two types of intramolecular hydrogen bonds are observed in Schiff bases: O–H $\cdots$ N in enol-imine<sup>17,18</sup> and N–H $\cdots$ O in keto-amine<sup>19,20</sup> tautomers. Different methods were used to show the presence of the enol-imine and keto-amine forms, among them UV–vis, IR, MS, <sup>1</sup>H, <sup>13</sup>C NMR spectroscopy, and X-ray crystallography techniques.<sup>21–24</sup>

Schiff base ligands consist of a variety of substituents with different electron-donating and electron-withdrawing groups and therefore may exhibit interesting electro-chemical properties. The Schiff base compounds have been also under investigation during past years because of their potential applicability in optical communications, and many of them have NLO behavior.<sup>25,26</sup> NLO materials have been attractive in recent years with respect to their future potential applications in the field of optoelectronic such as optical communication, optical computing, optical switching,

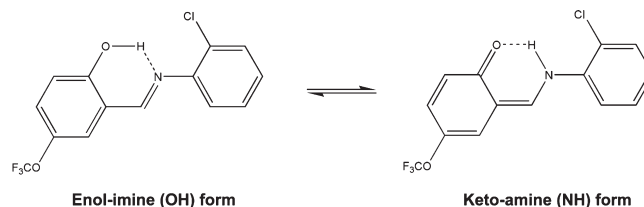


Figure 1. Tautomeric forms of the title compound.

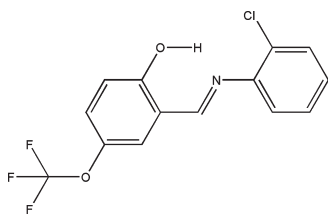
and dynamic image processing.<sup>27,28</sup> Because of their high molecular hyperpolarizabilities, organic materials display a number of significant nonlinear optical properties. NLO materials were categorized as multilayered semiconductor structures, molecular-based macroscopic assemblies, and traditional inorganic solids. A variety of inorganic, organic, and organometallic molecular systems have been studied for NLO activity.<sup>27,29</sup>

Currently, fluoro-containing organic compounds play an important role for the pharmaceutical as well as agrochemical industries, because of their often unique biological properties, such as the increased membrane permeability, enhanced hydrophobic binding, and stability against metabolic oxidation.<sup>30–35</sup> Among them, the trifluoromethylated molecules are of great significance and attract continuous attention from various fields.<sup>36–38</sup>

Received: June 20, 2011

Revised: October 13, 2011

Published: October 13, 2011

**Scheme 1. Chemical Diagram of (*E*)-2-[(2-Chlorophenyl)iminomethyl]-4-trifluoromethoxyphenol**

In recent years, density functional theory (DFT) has been the shooting star in theoretical modeling. The development of ever better exchange-correlation functionals has made it possible to calculate many molecular properties with accuracies comparable to those of traditional correlated ab initio methods, at more favorable computational costs.<sup>39</sup> Literature surveys have revealed the high degree of accuracy of DFT methods in reproducing the experimental values in terms of geometry, dipole moment, vibrational frequency, etc.<sup>40–43</sup>

The aim of this study is to investigate the energetic and structural properties of the Schiff base compound, (*E*)-2-[(2-chlorophenyl)iminomethyl]-4-trifluoromethoxyphenol (Scheme 1), using density functional theory calculations. In this study, the optimized geometry, vibrational spectra and assignments, statistical thermodynamic parameters, electronic absorption spectra, and nonlinear optical properties of the title compound have been studied. These calculations are valuable for providing insight into molecular properties of Schiff base compounds.

## 2. COMPUTATIONAL AND EXPERIMENTAL METHODS

**Physical Measurements.** The melting point was determined using a Gallenkamp melting point apparatus. The IR spectrum of the title compound was recorded in the range 4000–400  $\text{cm}^{-1}$  using a Schmadzu FTIR-8900 spectrophotometer with KBr pellets. Electronic absorption spectra were measured on a Unicam UV–vis spectrophotometer in EtOH.

**Synthesis.** The compound (*E*)-2-[(2-chlorophenyl)iminomethyl]-4-trifluoromethoxyphenol was prepared by refluxing a mixture of a solution containing 2-hydroxy-5-(trifluoromethoxy) benzaldehyde (0.027 g, 0.131 mmol) in 20 mL of ethanol and a solution containing 2-chloroaniline (0.017 g, 0.131 mmol) in 20 mL of ethanol. The reaction mixture was stirred for 1 h under reflux. The crystals of (*E*)-2-[(2-chlorophenyl)iminomethyl]-4-trifluoromethoxyphenol suitable for X-ray analysis were obtained from ethylalcohol by slow evaporation (yield: 73%; mp, 368 K).

**Crystal Structure Determination.** A light yellow crystal of the compound with dimensions of  $0.04 \times 0.18 \times 0.45$  mm was mounted on a goniometer of a STOE IPDS II diffractometer. Measurements were performed at room temperature (296 K) using graphite monochromated Mo  $K_{\alpha}$  radiation ( $\lambda = 0.71073$  Å). The systematic absences and intensity symmetries indicated the monoclinic *Pbca* space group. A total of 20 483 reflection (1080 unique) within the  $\theta$  range of  $[1.5^{\circ} < \theta < 26.5^{\circ}]$  were collected in the  $w$  scan mode. Cell parameters were determined by using X-AREA software.<sup>44</sup> The intensities collected were corrected for Lorentz and polarization factors, absorption correction ( $\mu = 0.32$   $\text{mm}^{-1}$ ), by the integration method via X-RED32 software.<sup>44</sup> The structure was solved by direct methods using

**Table 1. Crystallographic Data for the Title Compound**

chemical formula	$\text{C}_{14}\text{H}_9\text{ClF}_3\text{NO}_2$
crystal shape/color	needle/light yellow
formula weight	315.67
crystal system	orthorhombic
space group	<i>Pbca</i>
unit cell parameters	$a = 13.5727$ (7) Å $b = 7.5342$ (4) Å $c = 26.6045$ (17) Å
volume	$2720.6$ (3) Å <sup>3</sup>
Z	8
temperature	296 K
$D_x$ ( $\text{Mg cm}^{-3}$ )	1.541
$\mu$ ( $\text{mm}^{-1}$ )	0.32
$F_{000}$	1280
crystal size ( $\text{mm}^3$ )	$0.04 \times 0.18 \times 0.45$
data collection	
diffractometer/meas. meth	STOE IPDS II/ $w$ -scan
absorption correction	integration
$T_{\text{min}}$	0.8924
$T_{\text{max}}$	0.9894
no. of measured, independent, and observed reflections	20 483, 2823, 1080
criterion for observed reflections	$I > 2\sigma(I)$
$R_{\text{int}}$	0.179
$\theta_{\text{min}}, \theta_{\text{max}}$	$1.5^{\circ}, 26.5^{\circ}$
refinement	
refinement on	$F^2$
$R[F^2 > 2\sigma(F^2)], wR, S$	0.073, 0.069, 0.96
no. of reflection	2823
no. of parameters	194
weighting scheme	$w = 1/[\sigma^2(F_o^2) + (0.006P)^2]$ $P = (F_o^2 + 2F_c^2)/3$
$(\Delta/\sigma)_{\text{max}}$	0.001
$\Delta\rho_{\text{max}}, \Delta\rho_{\text{min}}$ ( $\text{e Å}^{-3}$ )	0.19, $-0.15$

SHELXS-97.<sup>45</sup> The maximum peaks and deepest hole observed in the final  $\Delta\rho$  map were 0.19 and  $-0.15$   $\text{e Å}^{-3}$ , respectively. The scattering factors were taken from SHELXL-97.<sup>45</sup> The molecular graphics were done using ORTEP-3 for Windows.<sup>46</sup> All non-hydrogen atoms were refined anisotropically. The refinement was carried out using the full matrix least-squares method on the positional and anisotropic temperature parameters of non-hydrogen atoms corresponding to 194 crystallographic parameters. Atom H1 was located in a difference Fourier map and refined isotropically, and the other H atoms were positioned geometrically and treated using a riding model, fixing the bond lengths at 0.93 Å for aromatic CH. The displacement parameters of the H atoms were fixed at  $U_{\text{iso}}(\text{H}) = 1.2U_{\text{eq}}(\text{C})$  of their parent atoms. Details of the data collection conditions and the parameters of the refinement process are given in Table 1.

**Computational Methods.** The DFT calculations with a hybrid functional B3LYP (Becke's three-parameter hybrid functional using the LYP correlation functional) at 6-311++G(d,p) basis set by the Berny method<sup>47,48</sup> were performed with the Gaussian 03W software package.<sup>49</sup> Geometry optimization was started from the X-ray experimental atomic position. The

molecular structure of the title compound in the ground state was optimized. For all of the calculations in this study, optimized structural parameters were used. The harmonic vibrational frequencies were calculated at the same level of theory for the optimized structure, and the obtained frequencies were scaled by 0.96. Vibrational band assignments were made using the Gauss-View molecular visualization program.<sup>50</sup> The vibrational frequency calculations at the same level of theory revealed no imaginary frequencies, indicating that an optimal geometry at this level of approximation was found for the title compound. The electronic absorption spectra were calculated using the time-dependent density functional theory (TD-DFT) method.<sup>51–54</sup> Also, it is calculated in ethanol solution using the Polarizable Continuum Model (PCM).<sup>55–58</sup> To investigate the tautomeric stability, some properties such as total energy, HOMO and LUMO energies, and the chemical hardness<sup>59</sup> for the OH and NH forms of the title compound were obtained at the 6-311++G(d,p) level in the gas phase. These properties were also examined for the title compound in solvent media with three kinds of solvent ( $\epsilon = 78.39$ , H<sub>2</sub>O;  $\epsilon = 24.55$ , C<sub>2</sub>H<sub>5</sub>OH;  $\epsilon = 4.9$ , CHCl<sub>3</sub>) using the PCM method. To investigate the reactive sites of the title compound, the MEP were evaluated using the B3LYP/6-31++G(d,p) method. MEP,  $V(r)$ , at a given point  $r(x,y,z)$  in the vicinity of a molecule, is defined in terms of the interaction energy between the electrical charge generated from the molecule's electrons and nuclei and a positive test charge (a proton) located at  $r$ . For the system studied, the  $V(r)$  values were calculated as described previously using the equation:<sup>60</sup>

$$V(r) = \sum_A \frac{Z_A}{|R_A - r|} - \int \frac{\rho(r')}{|r' - r|} dr' \quad (1)$$

where  $Z_A$  is the charge of nucleus  $A$ , located at  $R_A$ ,  $\rho(r')$  is the electronic density function of the molecule, and  $r'$  is the dummy integration variable. The first hyperpolarizability of the title compound was obtained by molecular polarizabilities based on theoretical calculations.

CCDC-810324 contains the supplementary crystallographic data for the compound reported in this Article. These data can be obtained free of charge at [www.ccdc.cam.ac.uk/conts/retrieving.html](http://www.ccdc.cam.ac.uk/conts/retrieving.html) [or from the Cambridge Crystallographic Data Centre (CCDC), 12 Union Road, Cambridge CB2 1EZ, UK; fax, +44(0)1223–336033; e-mail, [deposit@ccdc.cam.ac.uk](mailto:deposit@ccdc.cam.ac.uk)].

### 3. RESULTS AND DISCUSSION

**Description of the Crystal Structure.** The title compound, an Ortep-3 view of which is shown in Figure 2a, crystallizes in the orthorhombic space group  $Pbca$  with  $Z = 8$  in the unit cell. The asymmetric unit in the crystal structure contains only one molecule. The dihedral angle between the aromatic ring systems is  $2.9(2)^\circ$ . The imino group is coplanar with the hydroxyphenyl ring, as shown by the C9–C8–C7–N1 torsion angle of  $-2.5(7)^\circ$ . It is also known that Schiff bases may exhibit photochromism depending on the planarity or nonplanarity, respectively.<sup>61</sup>

The C7–N1 and C9–O1 bonds of the title compound are the most important indicators of the tautomeric type. The C9–O1 bond is of a double bond for the keto-amine tautomer, whereas this bond displays single bond character in the enol-imine tautomer. In addition, the C7–N1 bond is also a double bond in the enol-imine tautomer and of single bond length in the keto-amine tautomer.<sup>62</sup> In

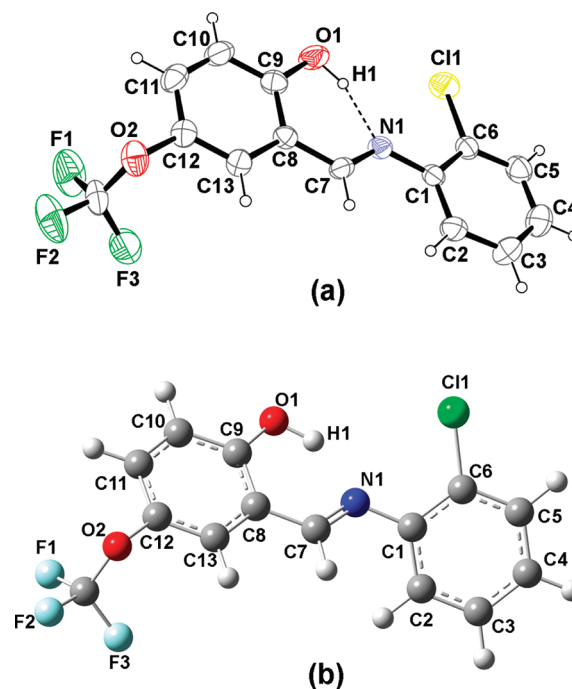


**Figure 2.** (a) Ortep-3 diagram of the title compound. Displacement ellipsoids are drawn at the 30% probability level, and H atoms are shown as small spheres of arbitrary radii. (b) The theoretical geometric structure of the title compound (B3LYP/6-31++G(d,p) level).

**Table 2. Hydrogen-Bond Geometry (Å, deg)**

D—H...A	D—H	H...A	D...A	D—H...A
X-ray				
O1—H1...N1	0.90 (3)	1.76 (4)	2.589 (4)	153 (4)
B3LYP/6-31++G(d,p)				
O1—H1...N1	0.99	1.75	2.639	145.93

the title compound, the enol-imine form is favored over the keto-amine form, as indicated by C9–O1 [1.343(5) Å] and C7–N1 [1.269(4) Å] bonds. The C9–O1 and C7–N1 bonds indicate single-bond and a high degree of double-bond characters, respectively. Similar results were observed for (*E*)-2-[(3-fluorophenyl)iminomethyl]-4-(trifluoromethoxy) phenol [C–O = 1.343(3) and C–N = 1.269(5) Å].<sup>63</sup>

The title compound is stabilized by O–H...N type hydrogen bond. There is a strong intramolecular O1–H1...N1 hydrogen bond involving hydroxyl atom O1 and imine atom N1, O1–H1...N1, producing an S(6) ring motif<sup>64</sup> resulting in approximate planarity of the molecular skeleton [O...N = 2.589(4) Å]. The details of the hydrogen bond are summarized in Table 2. In addition, there is also  $\pi$ – $\pi$  interaction between the Cg2 rings in a neighboring molecule of 3.768(3) Å at  $(\frac{1}{2} - x, -\frac{1}{2} + y, z)$  [Cg2 is the ring centroid of the C8/C13 ring]. A packing diagram of the title compound is shown in Figure 3.

**Optimized Geometry.** The optimized parameters (bond lengths, bond angles, and dihedral angles) of the title compound have been obtained using the B3LYP/6-31++G(d,p) method. The atomic numbering scheme and the theoretical geometric structure of the title compound are shown in Figure 2b. Calculated geometric parameters are listed in Table 3 along with the experimental data.

When the X-ray structure of the title compound is compared to its optimized counterparts (see Figure 4), slight conformational discrepancies are observed between them. The most remarkable discrepancy exists in the orientation of the chlorophenyl ring in the compound. The orientation of the chlorophenyl ring is defined by the torsion angles C2–C1–N1–C7 [ $179.8(4)^\circ$ ] and C6–C1–N1–C7 [ $0.1(6)^\circ$ ]. These torsion angles have been calculated at  $-142.30^\circ$  and  $40.99^\circ$  for the B3LYP/6-311++G(d,p) level, respectively. Another difference in the optimized structure is observed in the relative orientation of the trifluoromethoxy group. The methoxy group is almost perpendicular with the attached ring with C11–C12–O2–C14 and C13–C12–O2–C14 torsion angles of  $95.0(5)^\circ$  and  $-90.3(5)^\circ$  for X-ray, while the corresponding values are calculated as  $95.18^\circ$  and  $-89.12^\circ$  for B3LYP, respectively. According to X-ray studies, the dihedral angle between the C1/C6 and C8/C13 rings is  $2.9(2)^\circ$ , whereas the dihedral angle has been calculated at  $41.24^\circ$  for B3LYP. The geometry of hydrogen bond in the optimized structure is examined, and it is seen that for the O1–H1 $\cdots$ N1 hydrogen bond that exists between the phenol O1 atom and imine N1 atom, D–H, H $\cdots$ A, and D–H $\cdots$ A values are  $0.90(3)$  Å,  $1.76(4)$  Å, and  $153(4)^\circ$  for X-ray and  $0.99$  Å,  $1.75$  Å, and  $145.93^\circ$  for B3LYP, respectively. The presence of the H-bond appears as an important property of the molecule, stabilizing its conformation in the crystal; as shown in the molecular modeling part, this is also visible in the model obtained for the molecule discussed.

A logical method for globally comparing the structures obtained with the theoretical calculations is by superimposing the molecular skeleton with that obtained from X-ray diffraction, giving a RMSE of  $0.161$  Å for B3LYP/6-311++G(d,p) (Figure 4). This RMSE value is quite large. This magnitude of RMSE can be explained by the fact that the intermolecular Coulombic interaction with the neighboring molecules is absent in gas phase, whereas the experimental result corresponds to interacting molecules in the crystal lattice.

**IR Spectroscopy.** Harmonic vibrational frequencies of the title compound were calculated using the DFT/B3LYP method with the 6-311++G(d,p) basis set. The vibrational band assignments were made using the Gauss-View molecular visualization program. To facilitate assignment of the observed peaks, we have analyzed vibrational frequencies and compared our calculation results to the experimental ones and showed in Table 4. The agreement between the experimental and calculated frequencies is quite good in general.

The FT-IR spectrum of the title compound was recorded in the  $4000$ – $400$   $\text{cm}^{-1}$  region using KBr pellets on a Schmadzu FT-IR 8900 spectrophotometer and is given in Figure 5. The spectra contain some characteristic bands of the stretching vibrations of the O–H, C–H, C=N, C–O, C–Cl, and C–F groups. The O–H group gives rise to three vibrations as stretching, in-plane bending, and out-of-plane bending vibrations. The OH group vibrations are likely to be most sensitive to the environment, so they show pronounced shifts in the spectra of the hydrogen-bonded species. The non-hydrogen-bonded or a free hydroxyl group absorbs strongly in the  $3550$ – $3700$   $\text{cm}^{-1}$  region.<sup>65</sup> Intramolecular hydrogen bonding if present in the six-membered ring system would reduce the O–H stretching band to the  $3550$ – $3200$   $\text{cm}^{-1}$  region.<sup>66</sup> The IR spectrum of the title compound shows a band at  $3422$   $\text{cm}^{-1}$  due to O–H stretching vibration. This band has been calculated at  $3116$   $\text{cm}^{-1}$  for B3LYP. Generally, the OH in-plane bending vibration in phenols lies in the region  $1300$ – $1400$   $\text{cm}^{-1}$ .

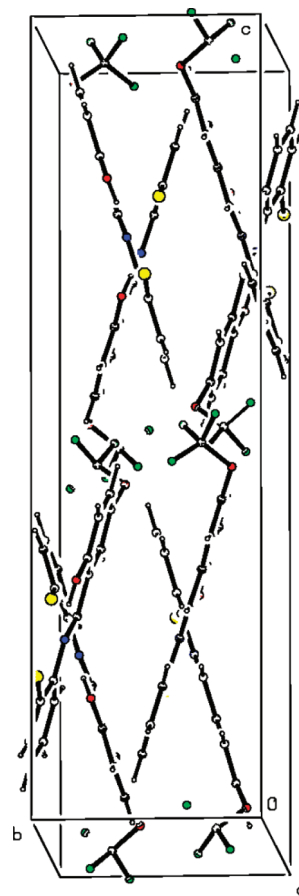


Figure 3. Packing diagram of the title compound.

The strong bands at  $1392$ – $1491$   $\text{cm}^{-1}$  in the FT-IR spectra correspond to in-plane bending vibration of the OH group. The OH out-of-plane deformation vibration in phenols, in general, lies in the region  $517$ – $710$   $\text{cm}^{-1}$ .<sup>67</sup> The band at  $829$   $\text{cm}^{-1}$  in the FT-IR spectra corresponds to out-of-plane bending mode of hydroxyl vibration. The calculated values of OH group vibrations show good agreement with the experimental results.

The aromatic C–H stretching, C–H in-plane bending, and C–H out-of-plane bending vibrations appear in  $2900$ – $3150$ ,  $1100$ – $1500$ , and  $750$ – $1000$   $\text{cm}^{-1}$  frequency ranges, respectively.<sup>68</sup> The C–H aromatic stretching mode was observed at  $3068$   $\text{cm}^{-1}$  experimentally and was calculated at  $3065$   $\text{cm}^{-1}$ . In addition, the aliphatic C–H stretching mode was observed at  $2922$   $\text{cm}^{-1}$ . The C–H in-plane bending vibrations assigned in the region  $1590$ – $1150$   $\text{cm}^{-1}$  are usually weak. The bands observed at  $965$ ,  $944$ ,  $889$ ,  $867$ ,  $757$ , and  $737$   $\text{cm}^{-1}$  in FT-IR spectra are assigned to the C–H out-of-plane bending vibration for the title compound.

The characteristic region of  $1500$ – $1700$   $\text{cm}^{-1}$  can be used to identify the proton transfer of Schiff bases. Azomethine (C=N) bond stretching vibration was observed to be  $1617$   $\text{cm}^{-1}$  experimentally, while it was calculated at  $1602$   $\text{cm}^{-1}$  for B3LYP. The bands observed at  $1617$ ,  $1590$ ,  $1571$ , and  $1542$   $\text{cm}^{-1}$ , which can be attributed to the C=C stretching vibrations, were calculated at  $1602$ ,  $1560$ ,  $1543$ , and  $1538$   $\text{cm}^{-1}$  for B3LYP, respectively. Another characteristic region of the Schiff bases derivative

Table 3. Selected Molecular Structure Parameters

parameters	experimental	B3LYP/6-311++G(d,p)
Bond Lengths (Å)		
C1–C2	1.379 (4)	1.405
C1–C6	1.384 (5)	1.403
C1–N1	1.405 (4)	1.402
C2–C3	1.382 (5)	1.389
C2–Cl1	1.733 (3)	1.752
C3–C4	1.376 (5)	1.392
C4–C5	1.372 (5)	1.393
C5–C6	1.377 (5)	1.390
C7–N1	1.269 (4)	1.286
C7–C8	1.446 (5)	1.450
C8–C9	1.401 (5)	1.420
C8–C13	1.408 (5)	1.406
C9–O1	1.343 (5)	1.337
C9–C10	1.395 (5)	1.402
C10–C11	1.367 (6)	1.384
C11–C12	1.369 (6)	1.395
C12–C13	1.351 (5)	1.378
C12–O2	1.420 (5)	1.411
C14–F2	1.304 (5)	1.333
C14–F1	1.308 (6)	1.350
C14–F3	1.311 (6)	1.352
C14–O2	1.316 (6)	1.348
Bond Angles (deg)		
C2–C1–C6	118.1 (3)	117.85
C2–C1–N1	116.2 (3)	119.64
C6–C1–N1	125.7 (4)	122.42
C1–C2–C3	121.7 (3)	121.20
C1–C2–Cl1	120.7 (3)	119.84
C3–C2–Cl1	117.6 (3)	118.94
C4–C3–C2	119.2 (4)	119.90
C5–C4–C3	119.8 (4)	119.88
C4–C5–C6	120.7 (4)	120.01
C5–C6–C1	120.4 (4)	121.13
N1–C7–C8	122.0 (4)	122.10
C9–C8–C13	118.2 (4)	119.14
C9–C8–C7	121.0 (4)	121.51
C13–C8–C7	120.9 (4)	119.34
O1–C9–C10	118.5 (4)	118.36
O1–C9–C8	121.9 (4)	122.21
C10–C9–C8	119.7 (4)	119.41
C11–C10–C9	120.1 (4)	120.54
C10–C11–C12	120.4 (4)	119.69
C13–C12–C11	121.0 (4)	121.14
C13–C12–O2	120.2 (4)	119.68
C11–C12–O2	118.6 (4)	119.02
C12–C13–C8	120.7 (4)	119.14
F2–C14–F1	107.4 (4)	108.32
F2–C14–F3	107.2 (5)	108.11
F1–C14–F3	104.7 (6)	106.57
F2–C14–O2	109.6 (5)	107.97
F1–C14–O2	114.0 (5)	112.88
F3–C14–O2	113.4 (4)	112.78

Table 3. Continued

parameters	experimental	B3LYP/6-311++G(d,p)
C7–N1–C1	123.7 (3)	121.11
C14–O2–C12	115.9 (4)	117.74
Torsion Angles (deg)		
C7–C8–C9–O1	−0.3 (7)	−0.29
C8–C7–N1–C1	179.9 (4)	−176.44
N1–C1–C2–Cl1	−1.5 (6)	2.85
F2–C14–O2–C12	−179.9 (4)	−178.54
F1–C14–O2–C12	−59.4 (6)	−58.81
F3–C14–O2–C12	60.3 (6)	62.06
C11–C12–O2–C14	95.0 (5)	95.18
C13–C12–O2–C14	−90.3 (5)	−89.12
C2–C1–N1–C7	179.8 (4)	−142.30
C6–C1–N1–C7	0.1 (6)	40.99

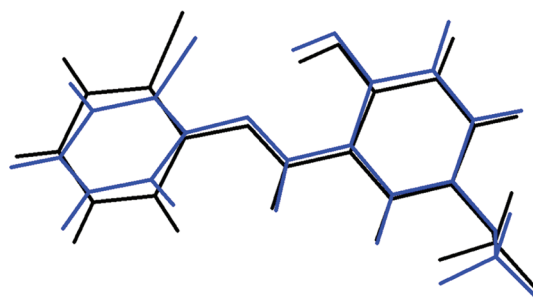


Figure 4. Atom-by-atom superimposition of the structures calculated (blue) over the X-ray structure (black) for the title compound.

spectrum is 1100–1400  $\text{cm}^{-1}$ , which is attributed to phenolic  $\text{C}_{\text{ar}}\text{--O}$  stretching vibrations. The  $\text{C}_{\text{ar}}\text{--O}$  stretching vibration was observed at 1293  $\text{cm}^{-1}$ , which confirms the presence of phenol group in the compound.

Three strong infrared bands at 1258, 1172, and 1150  $\text{cm}^{-1}$  are assigned to the C–F stretching modes. According to the calculations, the first two bands are caused by symmetric  $\text{CF}_3$  stretching modes, and the latter is due to the asymmetric  $\text{CF}_3$  stretching mode. Furthermore, the medium bands at 573 and 468  $\text{cm}^{-1}$  in the IR spectrum of the title compound are assigned to  $\text{CF}_3$  deformation modes. For simple organic chlorine compounds, C–Cl absorptions are in the region 1129–480  $\text{cm}^{-1}$ .<sup>69,70</sup> In the FT-IR spectrum of the title compound, a strong band at 684  $\text{cm}^{-1}$  is assigned to the C–Cl stretching vibration. The theoretical calculation by the B3LYP method at 690  $\text{cm}^{-1}$  exactly correlates with experimental observation. The above conclusions are in good agreement with the similar Schiff base compounds.<sup>71,72</sup> The other vibrational frequencies can be seen in Table 4.

As can be seen in Figure 1, the enol-imine form should have phenol O–H, azomethine C=N, and  $\text{C}_{\text{ar}}\text{--O}$  bonds. The presence of O–H, C=N, and C–O stretching vibrations in the FT-IR spectrum of the title compound strongly suggests that the title compound has the enol-imine form in the solid state.

**Electronic Absorption Spectra.** The UV–visible spectrum of *ortho*-hydroxylated Schiff bases that exist mainly as enol-imine structure indicates the presence of a band at <400 nm, while compounds that exist as keto-amine form show a new band, especially in polar and nonpolar solvents at >400 nm.<sup>73,74</sup>

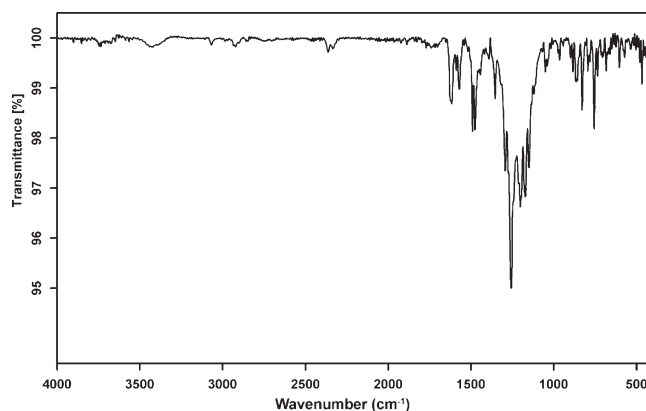
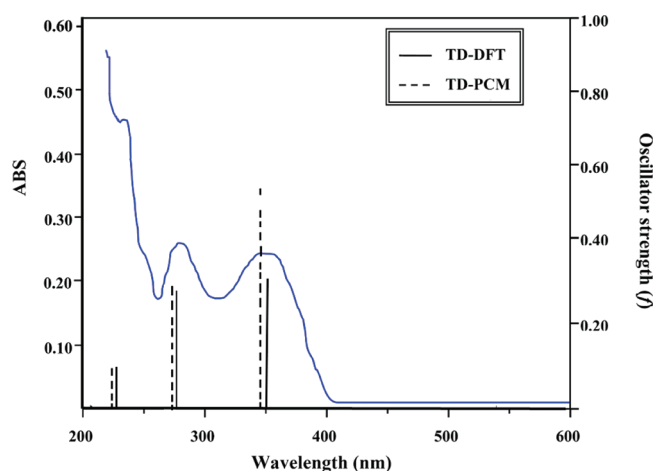
**Table 4.** Comparison of the Experimental and Calculated Vibrational Frequencies ( $\text{cm}^{-1}$ )

assignments <sup>a</sup>	experimental IR	
	with KBr	calculated
$\nu(\text{O-H})$	3422	3116
$\gamma_{\text{ring}}(\text{C-H})$ as	3068	3065
$\nu(\text{C-H})$ aliphatic	2922	2919
$\nu(\text{C=N}) + \nu(\text{C=C})$	1617	1602
$\nu(\text{C=C}) + \gamma_{\text{ring}}(\text{C-H})$	1590	1560
$\nu(\text{C=C}) + \gamma_{\text{ring}}(\text{C-H})$	1571	1543
$\nu(\text{C=C}) + \gamma_{\text{ring}}(\text{C-H})$	1542	1538
$\gamma(\text{OH}) + \gamma_{\text{ring}}(\text{C-H})$	1491	1457
$\gamma_{\text{ring}}(\text{C-H}) + \gamma(\text{C-H})$ aliphatic	1477	1445
$\gamma(\text{OH}) + \gamma_{\text{ring}}(\text{C-H})$	1444	1424
$\gamma_{\text{ring}}(\text{C-H})$	1419	1409
$\gamma(\text{OH}) + \gamma_{\text{ring}}(\text{C-H}) + \gamma(\text{CH})$ aliphatic	1392	1374
$\gamma_{\text{ring}}(\text{C-H}) + \gamma(\text{CH})$ aliphatic	1354	1330
$\nu(\text{C-O})$ phenol + $\gamma_{\text{ring}}(\text{C-H})$	1293	1265
$\nu(\text{C-F}_3)$ s + $\gamma_{\text{ring}}(\text{C-H})$	1258	1197
$\nu(\text{C-OCF}_3) + \gamma_{\text{ring}}(\text{C-H})$	1203	1174
$\nu(\text{O-CF}_3) + \gamma_{\text{ring}}(\text{C-H}) + \nu(\text{C-F}_3)$ s	1172	1150
$\gamma_{\text{ring}}(\text{C-H}) + \nu(\text{C-F}_3)$ as	1150	1084
$\omega_{\text{ring}}(\text{C-H}) + \omega(\text{C-H})$ aliphatic	965	963
$\delta_{\text{ring}}(\text{C-H})$	944	931
$\omega_{\text{ring}}(\text{C-H})$	889	872
$\omega_{\text{ring}}(\text{C-H})$	867	864
$\omega(\text{O-H})$	829	800
$\omega_{\text{ring}}(\text{C-H})$	757	734
$\omega_{\text{ring}}(\text{C-H})$	737	715
$\nu(\text{C-Cl})$	684	690
$\omega(\text{FCF}) \beta(\text{CCC})$	573	584
$\omega(\text{FCF}) + \beta(\text{OCC})$	468	478

<sup>a</sup>  $\nu$ , stretching;  $\alpha$ , scissoring;  $\gamma$ , rocking;  $\omega$ , wagging;  $\delta$ , twisting;  $\beta$ , bending; s, symmetric; as, asymmetric.

The electronic absorption spectra of the title compound in ethanol solvent were recorded within the 200–600 nm range, and a representative spectrum is shown in Figure 6. The experimentally observed spectra showed three bands at 348, 272, and 226 nm. These values are similar to those found in related Schiff base compounds.<sup>71,75</sup> The maximum absorption wavelength at 348 nm is assigned to intramolecular charge transfer band of the azomethine C=N group, which corresponds to the enol-imine form of the title compound. In this study, any band belonging to keto-amine form was not observed with a value greater than 400 nm, which indicates that the title compound is in the enol form and not in keto in ethanol solvent.

Electronic absorption spectra of the title compound were calculated by the TD-DFT method based on the B3LYP/6-311++G(d,p) level optimized structure in the gas phase. The calculated results are listed in Table 5 along with the experimental absorption spectra data. For TD-DFT calculations, the theoretical absorption bands are predicted at 350, 272, and 227 nm, and it can easily be seen that they correspond to the experimental absorption ones. In addition to the calculations in the gas phase, TD-DFT calculations of the title compound in ethanol solvent were performed by using the PCM model. The PCM calculations reveal that the calculated absorption bands have slight blue-shifts (see Figure 6) with values

**Figure 5.** FT-IR spectrum of the title compound.**Figure 6.** UV-vis spectra of the title compound in ethanol solvent and the comparison of calculated transitions in the gas phase and ethanol solvent with the experimental spectra.

of 349, 271, and 225 nm as compared to the gas-phase calculations of the TD-DFT method.

According to the investigation on the frontier molecular orbital (FMO) energy levels of the title compound, we can find that the corresponding electronic transfers happened between the highest occupied molecular orbital (HOMO) and the lowest unoccupied molecular orbital (LUMO), HOMO-3 and LUMO, HOMO and LUMO+3 orbitals, respectively. Figure 7 shows the distributions and energy levels of the FMOs computed at the B3LYP/6-311++G(d,p) level for the title compound. As was seen from Figure 7, in the HOMO-3 and LUMO, electrons are mainly delocalized on the chlorobenzene ring, trifluoromethoxyphenol fragment, and the atoms of imine group; in the HOMO and LUMO+3, electrons are delocalized on the whole structure. Molecular orbital coefficients analyses based on optimized geometry indicate that, for the title compound, the frontier molecular orbitals are mainly composed of p-atomic orbitals, so aforementioned electronic transitions are mainly derived from the contribution of bands  $\pi \rightarrow \pi^*$ .

**Energetics and Stability.** The NH and OH tautomerism of the title compound is given in Figure 1. To investigate the tautomeric stability, optimization calculations at B3LYP/6-311++G(d,p) level were performed for the NH and OH forms of the title compound. Some physicochemical properties such as total, HOMO, and

LUMO energies, dipole moment, and chemical hardness ( $\eta$ ) were also calculated with the same level of theory, and the results are given in Table 6. The chemical hardness is quite useful to rationalize the chemical stability and reactivity of chemical species. Also, the chemical hardness is quite useful to rationalize the relative stability and reactivity of chemical species. Hard species having a large HOMO–LUMO gap will be more stable and less reactive than soft species having a small HOMO–LUMO gap.<sup>76</sup> The hardness value of a molecule is formulated by eq 2:<sup>77</sup>

$$\eta = \frac{(-\varepsilon_{\text{HOMO}} + \varepsilon_{\text{LUMO}})}{2} \quad (2)$$

where  $\varepsilon_{\text{HOMO}}$  and  $\varepsilon_{\text{LUMO}}$  are the energies of the HOMO and LUMO orbitals. As seen from Table 6, the total energy of the OH form is lower than the NH form, while chemical hardness of the OH form is greater than the NH one, which indicates that the

**Table 5. Experimental and Theoretical Electronic Absorption Spectra Values**

experimental		TD-DFT		TD-PCM	
wavelength (nm)	abs	wavelength (nm)	oscillator strength	wavelength (nm)	oscillator strength
348	0.258	350	0.351	349	0.487
272	0.278	272	0.271	271	0.282
226	0.480	227	0.084	225	0.081

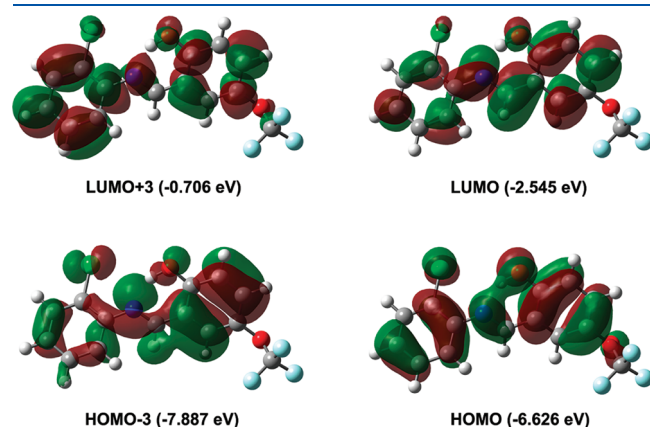


**Figure 7.** Molecular orbital surfaces and energy levels given in parentheses for the HOMO–3, HOMO–3, HOMO, LUMO, and LUMO +3 of the title compound computed at the B3LYP/6-311++G(d,p) level.

OH form of the title compound is more stable than its NH form in the gas phase.

To evaluate the solvent effect to the aforementioned properties of the title compound, calculations in three kinds of solvent ( $\varepsilon = 78.39$ , H<sub>2</sub>O;  $\varepsilon = 24.55$ , C<sub>2</sub>H<sub>5</sub>OH;  $\varepsilon = 4.9$ , CHCl<sub>3</sub>) were carried out with the B3LYP/6-311++G(d,p) level using the PCM model, and the results are given in Table 6. From Table 6, we can conclude that the total molecular energies obtained by PCM method decrease with the increasing polarity of the solvent, while the dipole moments and chemical hardness will increase with the increase of the polarity of the solvent.

**Molecular Electrostatic Potential.** Molecular electrostatic potential (MEP) is related to the electronic density and is a very useful descriptor in understanding sites for electrophilic attack and nucleophilic reactions as well as hydrogen-bonding interactions.<sup>78</sup> The electrostatic potential  $V(r)$  is also well suited for analyzing processes based on the “recognition” of one molecule by another, as in drug–receptor, and enzyme–substrate interactions, because it is through their potentials that the two species first “see” each other.<sup>79,80</sup>

To predict reactive sites for the electrophilic and nucleophilic process for the studied molecule, MEP surface was obtained at the B3LYP/6-311++G(d,p) optimized geometry. Following the approach reported previously,<sup>60</sup> we used those values of the MEP that correspond to the surface determined from points with electronic density  $\rho(r) = 0.001$  au. The negative (red and yellow) regions of MEP were related to electrophilic reactivity and the positive (blue) ones to nucleophilic reactivity shown in Figure 8. As can be seen in Figure 8, this molecule has several possible sites for electrophilic attack. Negative regions in the studied molecule were found around the phenol O1 atom, O2, Cl1, and fluor atoms of the CF<sub>3</sub> group. Also, a negative electrostatic potential region is observed around the N1 atom. The negative  $V(r)$  values are  $-0.041$  au for O1, which is the most negative region,  $-0.025$  au for O2,  $-0.015$  au for Cl1,  $-0.016$ ,  $-0.015$ , and  $-0.014$  au for F1, F2, and F3 atoms, respectively, and  $-0.006$  au for N1 atom, which is the least negative region. However, a maximum positive region is localized on the C7–H7 bond with a value of  $+0.044$  au, indicating a possible site for nucleophilic attack. According to these calculated results, the MEP map shows that the negative potential sites are on electronegative as well as the positive potential sites are around the hydrogen atoms. These sites give information about the region from where the compound can have noncovalent interactions.

**Nonlinear Optical Effects.** Nonlinear optical (NLO) effects arise from the interactions of electromagnetic fields in various media to produce new fields altered in phase, frequency, amplitude,

**Table 6. Calculated Energies, Dipole Moments, Frontier Orbital Energies, and Harnesses**

		gas phase ( $\varepsilon = 1$ )	chloroform ( $\varepsilon = 4.9$ )	ethanol ( $\varepsilon = 24.55$ )	water ( $\varepsilon = 78.39$ )
enol (OH) form	$E_{\text{TOTAL}}$ (hartree)	−1504.1621443	−1504.1732592	−1504.1777292	−1504.1788921
	$E_{\text{HOMO}}$ (eV)	−6.626	−6.522	−6.500	−6.493
	$E_{\text{LUMO}}$ (eV)	−2.545	−2.381	−2.346	−2.336
	$\eta$ (eV)	2.040	2.070	2.077	2.078
	$\mu$ (D)	3.116	4.000	4.419	4.513
keto (NH) form	$E_{\text{TOTAL}}$ (hartree)	−1504.1538606	−1504.1685945	−1504.1747781	−1504.1765508
	$E_{\text{HOMO}}$ (eV)	−6.108	−6.065	−6.076	−6.076
	$E_{\text{LUMO}}$ (eV)	−2.839	−2.709	−2.688	−2.677
	$\eta$ (eV)	1.634	1.678	1.694	1.699
	$\mu$ (D)	5.371	7.318	8.143	8.346

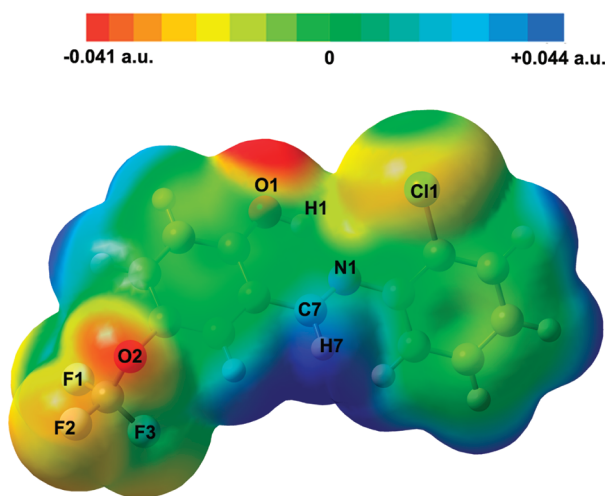


Figure 8. Molecular electrostatic potential map calculated at the B3LYP/6-311++G(d,p) level.

Table 7. Comparison of the Calculated  $\beta_{\text{tot}}$  Values with the Experimental  $\beta_{\text{tot}}$  Values in Units of  $10^{-30}$  esu

molecule	experimental <sup>a</sup>	6-31 6-31G(d)	6-31 +G(d)	6-311 ++G(d,p)	6-311 +G(d)	6-311 ++G(d,p)
urea	0.45	0.37	0.49	0.75	0.62	0.77
MNA <sup>b</sup>	16	11.54	14.99	14.33	14.60	13.93
PNA <sup>c</sup>	16.2	11.43	14.86	14.66	14.60	14.39

<sup>a</sup> Experimental data from refs 91 and 92. <sup>b</sup> 2-Methyl-4-nitroaniline. <sup>c</sup> *p*-Nitroaniline.

or other propagation characteristics from the incident fields.<sup>81</sup> NLO is at the forefront of current research because of its importance in

$$\beta_{\text{tot}} = \sqrt{(\beta_{xxx} + \beta_{xyy} + \beta_{xzz})^2 + (\beta_{yyy} + \beta_{yzz} + \beta_{yxx})^2 + (\beta_{zzz} + \beta_{zxx} + \beta_{zyy})^2} \quad (7)$$

The calculations of the total molecular dipole moment ( $\mu$ ), linear polarizability ( $\alpha$ ), and first-order hyperpolarizability ( $\beta$ ) from the Gaussian output have been explained in detail previously.<sup>88</sup> It is well-known that from the literature, the B3LYP approach provides fairly reliable values in electric hyperpolarizability calculations when compared to accuracies of traditional ab initio methods, and this predictive capability of widely used B3LYP method is of interest to a wide audience of computational scientists.<sup>89,90</sup> To investigate the effects of basis sets on the NLO properties, the  $\beta_{\text{tot}}$  values of urea, *p*-nitroaniline, and 2-methyl-4-nitroaniline were calculated by the B3LYP method with 6-31G(d), 6-31+G(d), 6-31++G(d,p), 6-311+G(d), and 6-311++G(d,p) basis sets, and the obtained results were compared to the experimental ones and given in Table 7. From this table, we see that calculated values of the  $\beta_{\text{tot}}$  slightly depend on the size of basis sets. Obtained values of the  $\beta_{\text{tot}}$  with 6-31G(d) basis set are smaller than those obtained with a large size of basis sets. It is found that the calculated results for the basis sets from 6 to 31+G(d) to 6-311++G(d,p) have minor differences from each other. The 6-31+G(d) basis set seems to be adequate for reproducing the hyperpolarizabilities. Taking into

providing the key functions of frequency shifting, optical modulation, optical switching, optical logic, and optical memory for the emerging technologies in areas such as telecommunications, signal processing, and optical interconnections.<sup>82–85</sup>

The nonlinear optical response of an isolated molecule in an electric field  $E_i(\omega)$  can be presented as a Taylor series expansion of the total dipole moment,  $\mu_{\text{tot}}$  induced by the field:

$$\mu_{\text{tot}} = \mu_0 + \alpha_{ij}E_j + \beta_{ijk}E_jE_k + \dots \quad (3)$$

where  $\alpha$  is the linear polarizability,  $\mu_0$  is the permanent dipole moment and  $\beta_{ijk}$  are the first hyperpolarizability tensor components. The isotropic (or average) linear polarizability is defined as:<sup>86</sup>

$$\alpha_{\text{tot}} = \frac{\alpha_{xx} + \alpha_{yy} + \alpha_{zz}}{3} \quad (4)$$

First hyperpolarizability is a third rank tensor that can be described by  $3 \times 3 \times 3$  matrix. The 27 components of 3D matrix can be reduced to 10 components due to the Kleinman symmetry<sup>87</sup> ( $\beta_{xyy} = \beta_{yxy} = \beta_{yyx} = \beta_{yyz} = \beta_{yzy} = \beta_{zyy}$ ; likewise other permutations also take same value). The output from Gaussian 03 provides 10 components of this matrix as  $\beta_{xxx}$ ,  $\beta_{xxy}$ ,  $\beta_{xyy}$ ,  $\beta_{yyy}$ ,  $\beta_{xxz}$ ,  $\beta_{xyz}$ ,  $\beta_{yyz}$ ,  $\beta_{zzz}$ ,  $\beta_{yzz}$ , and  $\beta_{zzz}$ , respectively. The components of the first hyperpolarizability can be calculated using the following equation:<sup>86</sup>

$$\beta_i = \beta_{iii} + \frac{1}{3} \sum_{i \neq j} (\beta_{ijj} + \beta_{jij} + \beta_{jji}) \quad (5)$$

Using the  $x$ ,  $y$ , and  $z$  components of  $\beta$ , the magnitude of the first hyperpolarizability tensor can be calculated by:

$$\beta_{\text{tot}} = \sqrt{(\beta_x^2 + \beta_y^2 + \beta_z^2)} \quad (6)$$

The complete equation for calculating the magnitude of  $\beta$  from Gaussian 03W output is given as follows:

account reliability and the computational time required, the basis set 6-31+G(d) was chosen for the calculations of the hyperpolarizabilities in this study.

The  $\beta_{\text{tot}}$  of the title compound was calculated at the B3LYP/6-31+G(d) level using the Gaussian 03W program package. The calculated value of  $\beta_{\text{tot}}$  is  $3.985 \times 10^{-30}$  esu, which is greater than that of urea (the  $\beta_{\text{tot}}$  of urea is  $0.49 \times 10^{-30}$  esu obtained by the B3LYP/6-31+G(d) method). When it is compared to the similar Schiff base compound in the literature, the calculated value of  $\beta_{\text{tot}}$  of the title compound is bigger than that of 3-[(1*E*)-*N*-ethylethanimidoyl]-4-hydroxy-6-methyl-2*H*-pyran-2-one ( $\beta_{\text{tot}} = 1.002 \times 10^{-30}$  esu).<sup>29</sup> These results indicate that the title compound is a good candidate of NLO material.

To understand this phenomenon in the context of molecular orbital theory, we examined the molecular HOMOs and molecular LUMOs of the title compound. The HOMO–LUMO energy gaps were calculated as 4.024 eV for the title compound, 4.666 eV for 3-[(1*E*)-*N*-ethylethanimidoyl]-4-hydroxy-6-methyl-2*H*-pyran-2-one,<sup>29</sup> and 6.891 eV for urea by the B3LYP/6-31+G(d) method.

**Table 8.** Total Energies ( $\text{kJ mol}^{-1}$ ), Zero-Point Energies ( $\text{kJ mol}^{-1}$ ), and Thermodynamic Properties of the Reactants and Title Compound at Different Temperatures

structure	temperature (K)	$H_m^0$ ( $\text{kJ mol}^{-1}$ )	$C_{p,m}^0$ ( $\text{J mol}^{-1} \text{K}^{-1}$ )	$S_m^0$ ( $\text{J mol}^{-1} \text{K}^{-1}$ )
Reactants				
TBA <sup>a</sup>	200	16.884	131.796	390.944
	250	24.606	160.284	425.286
	298.15	33.359	186.472	457.244
	300	33.721	187.447	458.453
	350	44.147	212.597	490.544
	400	55.773	235.341	521.556
	450	68.473	255.575	551.451
	500	82.123	273.420	580.195
	ZPE	309.346		
	E	-2 187 193.272		
CA <sup>b</sup>	200	10.583	78.592	304.662
	250	15.416	97.993	326.142
	298.15	20.972	116.068	346.426
	300	21.203	116.746	347.196
	350	27.901	134.281	367.811
	400	35.436	150.272	387.915
	450	43.732	164.611	407.437
	500	52.704	177.359	426.328
	ZPE	270.533		
	E	-1 961 772.502		
Products				
H <sub>2</sub> O	200	6.652	24.953	175.552
	250	8.284	24.999	182.978
	298.15	9.916	25.129	188.857
	300	9.957	25.137	189.062
	350	11.631	25.384	194.238
	400	13.346	25.735	198.760
	450	15.070	26.166	202.794
	500	16.805	26.660	206.451
	ZPE	53.426		
	E	-200 611.847		
title compound	200	24.981	202.175	502.795
	250	36.631	247.081	554.597
	298.15	49.944	289.026	603.203
	300	50.498	290.591	605.044
	350	66.472	331.226	654.218
	400	84.388	368.141	701.995
	450	104.051	401.065	748.287
	500	125.262	430.144	792.981
	ZPE	518.987		
	E	-3 949 180.477		

<sup>a</sup> 2-Hydroxy-5-(trifluoromethoxy)benzaldehyde. <sup>b</sup> 2-Chloroaniline.

As can be seen from the  $\beta_{\text{tot}}$  values for these compounds, there is an inverse relationship between first hyperpolarizability and HOMO–LUMO gap, allowing the molecular orbitals to overlap to have a proper electronic communication conjugation, which is a marker of the intramolecular charge transfer from the electron-donating group through the  $\pi$ -conjugation system to the electron-accepting group.<sup>93,94</sup>

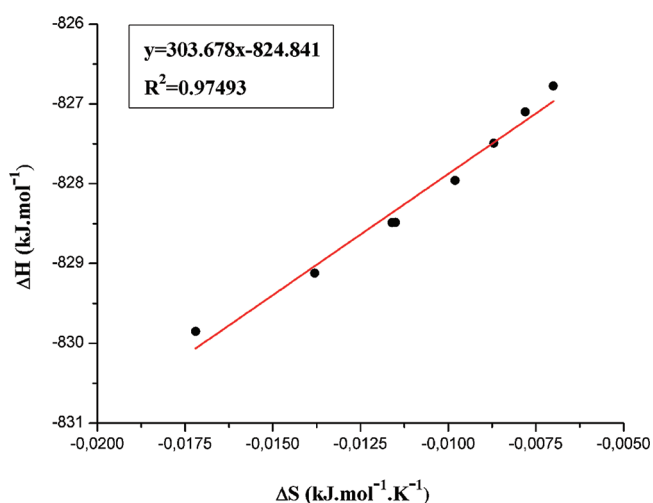
**Table 9.** Enthalpy, Entropy, and Free Energy Changes of the Formation Reaction of the Title Compound at the Different Temperatures

temperature (K)	$\Delta S$ ( $\text{kJ mol}^{-1} \text{K}^{-1}$ ) <sup>a</sup>	$\Delta H$ ( $\text{kJ mol}^{-1}$ ) <sup>b</sup>	$\Delta G$ ( $\text{kJ mol}^{-1}$ ) <sup>c</sup>
200	-0.0172	-829.850	-826.410
250	-0.0138	-829.123	-825.673
298.15	-0.0116	-828.487	-825.028
300	-0.0115	-828.485	-825.035
350	-0.0098	-827.961	-824.531
400	-0.0087	-827.491	-824.011
450	-0.0078	-827.100	-823.590
500	-0.0070	-826.776	-823.276

$$^a \Delta S = (S_m^0)_{\text{title compound}} + (S_m^0)_{\text{H}_2\text{O}} - (S_m^0)_{\text{TBA}} - (S_m^0)_{\text{CA}}$$

$$^b \Delta H = (H_m^0 + E + ZPE)_{\text{title compound}} + (H_m^0 + E + ZPE)_{\text{H}_2\text{O}} - (H_m^0 + E + ZPE)_{\text{TBA}} - (H_m^0 + E + ZPE)_{\text{CA}}$$

$$^c \Delta G = \Delta H - T\Delta S$$

**Figure 9.** Plot of the enthalpy versus entropy values for the formation reaction of the title compound.

**Thermodynamic Properties.** To determine thermodynamical properties of the title compound, the standard thermodynamic functions, heat capacity ( $C_{p,m}^0$ ), entropy ( $S_m^0$ ), and enthalpy ( $H_m^0$ ) based on the vibrational analysis at B3LYP/6-311++G(d,p) level and statistical thermodynamics for each of the reactants and products in the formation reaction of the title compound, were obtained and are listed in Table 8. The scale factor for frequencies is 0.96, which is used for an accurate prediction in determining the thermodynamic functions.

As can be seen from Table 8, the standard heat capacities, entropies, and enthalpies increase at any temperature from 200.00 to 500.00 K, because the intensities of molecular vibration increase with the increasing temperature. The enthalpy change ( $\Delta H$ ) and the entropy change ( $\Delta S$ ) for the formation reaction of the title compound are also obtained and listed in Table 9. In the course of formation of the title compound, the calculated  $\Delta S$  and the  $\Delta H$  decrease at any temperature from 200 to 500 K. Hence, the formation of title compound is an exothermic process that is accompanied by a decrease in the entropy. Using the  $\Delta G = \Delta H - T\Delta S$  equation,

the change of Gibbs free energy ( $\Delta G$ ) at various temperatures was also obtained (see Table 9).

One of the ways of getting the most stable tautomer is to calculate the tautomeric equilibrium constant,  $K_T$ , which is readily calculated from the Gibb's free energy via  $K_T = e^{-\Delta G/RT}$ , where  $\Delta G$  is the change in Gibb's free energy between products and reactants at temperature  $T$  and  $R$  is the ideal gas constant.<sup>95</sup> The  $\Delta G$  value at the B3LYP/6-311++G(d,p) level is predicted to be 19.475 kJ/mol between enol-imine and keto-amine tautomers of the title compound. The  $K_T$  is computed as  $3.85 \times 10^{-4}$  at 298.15 K for enol $\leftrightarrow$ keto tautomerization. This observation indicates that the direction of equilibrium is in favor of the enol structure.

Moreover, the linear relationship between  $\Delta H$  and  $\Delta S$  values, which is known as enthalpy–entropy compensation (EEC),<sup>96</sup> was also examined. Using the thermodynamical data from Table 9, the correlation between  $\Delta H$  and  $\Delta S$  is presented in Figure 9. As shown in Figure 9, an acceptable linear relationship between  $\Delta H$  and  $\Delta S$  for the formation reaction of the title compound is observed.

The graph of enthalpy versus entropy values for this reaction generates a quite linear trend and can be expressed by  $\Delta H = T_c \Delta S + b$  ( $T_c$  = compensation temperature and  $b$  = compensation free enthalpy), with  $T_c = 303.678 \pm 18.373$  K and  $b = -824.841 \pm 0.208$  kJ/mol. At this temperature, any variation in the standard enthalpy in different temperatures is balanced by a compensating variation in the standard entropy,<sup>97,98</sup> such that the  $\Delta G$  of the reaction (the  $y$  intercept of the plot) remains constant at  $b = -824.841$  kJ/mol.

To test the reality of EEC correlation, the Starikov and Norden EEC model can be applied,<sup>99</sup> suggesting that if the EEC is a statistically significant and physically nontrivial correlation, the hidden Carnot process may be represented by a set of microscopic heat engines, depending on the relation between the experimental temperature  $T$ , which is the temperature at which the phase transition takes place, and the compensation temperature,  $T_c$ ;  $T_c > T$  (“heat pump”) and  $T_c < T$  (“refrigerator”). The experimental temperature in the formation reaction of the title compound is about 350 K, which is bigger than the observed  $T_c$  ( $303.678 \pm 18.373$  K). According to our interpretation, the formation reaction of the title compound can then be described in terms of an artificial refrigerator model.

According to the data in Table 8 for the title compound, the correlations between the thermodynamic properties  $C_{p,m}^0$ ,  $S_m^0$ , and  $H_m^0$  and temperatures  $T$  are described. On the basis of these relationships, the values of  $C_{p,m}^0$ ,  $S_m^0$ , and  $H_m^0$  can be obtained at any other temperature. The correlation equations of the title compound are as follows:

$$C_{p,m}^0 = -17.2272 + 1.22489T - 6.58119 \times 10^{-5}T^2 \quad (R^2 = 0.99991) \quad (8)$$

$$S_m^0 = 281.11283 + 1.16416T - 2.80468 \times 10^{-4}T^2 \quad (R^2 = 1) \quad (9)$$

$$H_m^0 = -3.6859 + 0.06523T + 3.86119 \times 10^{-4}T^2 \quad (R^2 = 0.99997) \quad (10)$$

#### 4. CONCLUSIONS

(*E*)-2-[(2-Chlorophenyl)iminomethyl]-4-trifluoromethoxyphenol has been synthesized and characterized by IR, UV–vis,

and X-ray single-crystal diffraction. The X-ray, IR, and UV–vis spectral data for the title compound show that the compound exists in the enol form, which is stabilized by the intramolecular O–H $\cdots$ N hydrogen bond. FT-IR spectra analyses show that the predicted vibrational frequencies are in good agreement with the experimental values. The TD-DFT calculations lead to a very closer agreement with the experimental absorption spectra both in the gas phase and in solvent media. Molecular orbital coefficients analyses reveal that the electronic transitions are mainly assigned to  $\pi \rightarrow \pi^*$  electronic transitions. The MEP map shows that the negative potential sites are on electronegative atoms while the positive potential sites are around the hydrogen atoms. These sites give information about the region from where the compound can have noncovalent interactions. The nonlinear optical properties are also addressed theoretically. The predicted NLO properties of the title compound are much greater than ones of urea. The title compound is a good candidate as second-order NLO material. The values of  $\Delta G$  of the title compound formation became more positive as temperature increases. At 298.15 K, the change of  $\Delta G$  for the formation reaction of the title compound is  $-824.841$  kJ/mol. The title compound can spontaneously be produced from the isolated monomers at room temperature. The tautomeric equilibrium constant is computed as  $3.85 \times 10^{-4}$  at 298.15 K for enol $\leftrightarrow$ keto tautomerization of the title compound. It is shown that the enol form is strongly preferred over the keto form of the title compound. The enthalpy–entropy compensation effect has been observed for the formation reaction of the title compound, and the compensation temperature is reported. Analysis performed within the framework of the Starikov and Norden EEC model shows that the  $T_c$  is smaller than the average experimental temperature. Thus, the compensation behavior between  $\Delta H$  and  $\Delta S$  for the formation reaction of the title compound may be described in terms of an artificial refrigerator model. I hope this Article will be helpful for the design and synthesis of new materials.

#### AUTHOR INFORMATION

##### Corresponding Author

\*Tel.: +90 358 218 01 60. Fax: +90 358 218 01 04. E-mail: hasantanak@gmail.com.

#### ACKNOWLEDGMENT

I thank Professor Orhan Büyükgüngör for his help with the data collection and Associate Professor Ayşen Ağar for helping with the synthesized crystal, and I acknowledge the Faculty of Arts and Sciences, Ondokuz Mayıs University, Department of Physics, Turkey, for access to the Gaussian 03W program package.

#### REFERENCES

- (1) Emregul, K. C.; Duzgun, E.; Atakol, O. *Corros. Sci.* **2006**, *48*, 3243–3260.
- (2) Drozdak, R.; Allaert, B.; Ledoux, N.; Dragutan, I.; Dragutan, V.; Verpoort, R. *Coord. Chem. Rev.* **2005**, *249*, 3055–3074.
- (3) Sessler, J. L.; Melfi, P. J.; Dan Pantos, G. *Coord. Chem. Rev.* **2006**, *250*, 816–843.
- (4) Yang, C. J.; Jenekhe, S. A. *Macromolecules* **1995**, *28*, 1180–1196.
- (5) Destri, S.; Khotina, I. A.; Porzio, W. *Macromolecules* **1998**, *31*, 1079–1086.
- (6) Ggrigoras, M.; Catanescu, O.; Simonescu, C. I. *Rev. Roum. Chim.* **2001**, *46*, 927–939.

- (7) Kaya, I.; Vilayetoglu, A. R.; Mart, H. *Polymer* **2001**, *42*, 4859–4865.
- (8) Larkin, D. R. *J. Org. Chem.* **1990**, *55*, 1563–1568.
- (9) Vanco, J.; Svajlenova, O.; Racanska, E.; Muselik, J.; Valentova, J.; Trace, J. *Elem. Med. Biol.* **2004**, *18*, 155–161.
- (10) Jarzabek, B.; Kaczmarczyk, B.; Sek, D. *Spectrochim. Acta, Part A* **2009**, *74*, 949–954.
- (11) Cohen, M. D.; Schmidt, G. M. J.; Flavian, S. *J. Chem. Soc.* **1964**, 2041–2051.
- (12) Hadjoudis, E.; Vitterakis, M.; Mavridis, I. M. *Tetrahedron* **1987**, *43*, 1345–1360.
- (13) Xu, X. X.; You, X. Z.; Sun, Z. F.; Wang, X.; Liu, H. X. *Acta Crystallogr., Sect. C* **1994**, *50*, 1169–1171.
- (14) Feringa, L.; Jager, W. F.; De Lange, B. *Tetrahedron* **1993**, *49*, 8267–8310.
- (15) Schaumburg, K.; Lehn, J. M.; Goulle, C.; Roth, S.; Byrne, H.; Hagen, S.; Poplawsky, J.; Brufeldt, K.; Beechgard, K.; Pjornholm, T.; et al. In *Nanostructure Based Molecular Materials*; Göpel, W., Ziegler, C., Eds.; Wiley-VCH: Weinheim, Germany, 1992.
- (16) Willner, I.; Rubin, S. *Angew. Chem., Int. Ed. Engl.* **1996**, *35*, 367–385.
- (17) Tanak, H.; Erşahin, F.; Agar, E.; Yavuz, M.; Büyükgüngör, O. *Acta Crystallogr., Sect. E* **2009**, *65*, o2291.
- (18) Özek, A.; Albayrak, C.; Odabaşoğlu, M.; Büyükgüngör, O. *Acta Crystallogr., Sect. C* **2007**, *63*, o177.
- (19) Ünver, H.; Kabak, M.; Mehmet Zengin, D.; Nuri Durlu, T. *J. Chem. Crystallogr.* **2001**, *31*, 203–209.
- (20) Yavuz, M.; Tanak, H. *J. Mol. Struct. (THEOCHEM)* **2010**, *961*, 9–16.
- (21) Ünver, H. *Spectrosc. Lett.* **2001**, *34*, 783–791.
- (22) Salman, S. R.; Lindon, J. C.; Farrant, R. D. *Magn. Reson. Chem.* **1993**, *31*, 991–994.
- (23) Alarcon, S. H.; Olivieri, A. C.; Nordon, A. *Tetrahedron* **1995**, *51*, 4619–4626.
- (24) Kosar, B.; Özek, A.; Albayrak, C.; Büyükgüngör, O. *Acta Crystallogr., Sect. E* **2010**, *66*, o469.
- (25) Jalali-Heravi, M.; Khandar, A. A.; Sheikshoae, I. *Spectrochim. Acta, Part A* **1999**, *55*, 2537–2544.
- (26) Ünver, H.; Karakaş, A.; Elmali, A. *J. Mol. Struct.* **2004**, *702*, 49–54.
- (27) Kanis, D. R.; Ratner, M. A.; Marks, T. *Chem. Rev.* **1994**, *94*, 195.
- (28) Prasad, P. N.; Williams, D. J. *Introduction to Nonlinear Optical Effects in Molecules and Polymers*; Wiley: New York, 1991.
- (29) Avcı, D.; Basoğlu, A.; Atalay, Y. *Struct. Chem.* **2010**, *21*, 213–219.
- (30) Kirk, K. L. *J. Fluorine Chem.* **2006**, *127*, 1013–1029.
- (31) Chambers, R. D.; Holling, D.; Sandford, G.; Batsanov, A. S.; Howard, J. A. K. *J. Fluorine Chem.* **2004**, *125*, 661–671.
- (32) Ramachandran, P. V. *Proceedings of the ACS Symposium Series*; American Chemical Society: Washington, DC, 2000.
- (33) Himaya, T. *Organofluorine Compounds*; Springer-Verlag: Berlin, Heidelberg, 2001.
- (34) Kirsch, P. *Modern Fluoroorganic Chemistry: Synthesis, Reactivity and Applications*; Wiley-VCH: New York, Heidelberg, 2004.
- (35) Ojima, I.; McCarthy, J. R.; Welch, J. T. *Biomedical Frontiers of Fluorine Chemistry*; American Chemical Society: Washington, DC, 1996.
- (36) Quan, M. L.; Lam, P. Y. S.; Han, Q.; Pinto, D. J. P.; He, M. Y.; Li, R. H.; Ellis, C. D.; Clark, C. A.; Sun, J. H.; Alexander, R. S.; et al. *J. Med. Chem.* **2005**, *48*, 1729–1744.
- (37) Khudina, O. G.; Shchegolkov, E. V.; Burgart, Y. V.; Kodess, M. I.; Kazheva, O. N.; Chekhlov, A. N.; Shilov, G. V.; Dyachenko, O. A.; Saloutin, V. I.; Chupakhin, O. N. *J. Fluorine Chem.* **2005**, *126*, 1230–1238.
- (38) Schlosser, M.; Volle, J. N.; Leroux, F.; Schenk, K. *Eur. J. Org. Chem.* **2002**, 2913–2920.
- (39) Proft, F. D.; Geerlings, P. *Chem. Rev.* **2001**, *101*, 1451–1464.
- (40) Kurt, M.; Sertbakan, T. R.; Ozduran, M. *Spectrochim. Acta, Part A* **2008**, *70*, 664.
- (41) Jian, F. F.; Zhao, P. S.; Bai, Z. S.; Zhang, L. *Struct. Chem.* **2005**, *16*, 635.
- (42) Tanak, H.; Erşahin, F.; Köysal, Y.; Ağar, E.; Işık, Ş.; Yavuz, M. *J. Mol. Model.* **2009**, *15*, 1281–1290.
- (43) Ağar, A. A.; Tanak, H.; Yavuz, M. *Mol. Phys.* **2010**, *108*, 1759–1772.
- (44) Stoe and Cie. *X-Area (Version 1.18) and X-RED32 (Version 1.04)*; Stoe & Cie: Darmstadt, Germany, 2002.
- (45) Sheldrick, G. M. *SHELXS97 and SHELXL97*; University of Göttingen: Germany, 1997.
- (46) Farrugia, L. J. ORTEP-3 for Windows. *J. Appl. Crystallogr.* **1997**, *30*, 565.
- (47) Schlegel, H. B. *J. Comput. Chem.* **1982**, *3*, 214–218.
- (48) Peng, C.; Ayala, P. Y.; Schlegel, H. B.; Frisch, M. J. *J. Comput. Chem.* **1996**, *17*, 49–56.
- (49) Frisch, M. J.; Trucks, G. W.; Schlegel, H. B.; Scuseria, G. E.; Robb, M. A.; Cheeseman, J. R.; Montgomery, J. A., Jr.; Vreven, T.; Kudin, K. N.; Burant, J. C.; et al. *Gaussian 03*; Gaussian, Inc.: Wallingford, CT, 2004.
- (50) Dennington, R., II; Keith, T.; Millam, J. *GaussView, Version 4.1.2*; Semichem, Inc.: Shawnee Mission, KS, 2007.
- (51) Runge, E.; Gross, E. K. U. *Phys. Rev. Lett.* **1984**, *52*, 997–1000.
- (52) Stratmann, R. E.; Scuseria, G. E.; Frisch, M. J. *J. Chem. Phys.* **1998**, *109*, 8218–8224.
- (53) Bauernschmitt, R.; Ahlrichs, R. *Chem. Phys. Lett.* **1996**, *256*, 454–464.
- (54) Casida, M. E.; Jamorski, C.; Casida, K. C.; Salahub, D. R. *J. Chem. Phys.* **1998**, *108*, 4439–4449.
- (55) Miertus, S.; Scrocco, E.; Tomasi, J. *Chem. Phys.* **1981**, *55*, 117–129.
- (56) Barone, V.; Cossi, M. *J. Phys. Chem. A* **1998**, *102*, 1995–2001.
- (57) Cossi, M.; Rega, N.; Scalmani, G.; Barone, V. *J. Comput. Chem.* **2003**, *24*, 669–681.
- (58) Tomasi, J.; Mennucci, B.; Cammi, R. *Chem. Rev.* **2005**, *105*, 2999–3093.
- (59) Parr, R. G.; Pearson, R. G. *J. Am. Chem. Soc.* **1983**, *105*, 7512.
- (60) Politzer, P.; Murray, J. *Theor. Chem. Acc.* **2002**, *108*, 134–142.
- (61) Moustakali-Mavridis, I.; Hadjoudis, E.; Mavridis, A. *Acta Crystallogr., Sect. B* **1978**, *34*, 3709–3715.
- (62) Petek, H.; Albayrak, Ç.; Odabaşoğlu, M.; Şenel, I.; Büyükgüngör, O. *J. Chem. Crystallogr.* **2008**, *38*, 901–905.
- (63) Alpaslan, Y. B.; Alpaslan, G.; Ağar, A.; Işık, Ş. *Acta Crystallogr., Sect. E* **2010**, *66*, o510.
- (64) Bernstein, J.; Davies, R. E.; Shimon, L.; Chang, N. L. *Angew. Chem., Int. Ed. Engl.* **1995**, *34*, 1555–1573.
- (65) Teimouri, A.; Chermahini, A. N.; Taban, K.; Dabbagh, H. A. *Spectrochim. Acta, Part A* **2009**, *72*, 369–377.
- (66) Dabbagh, H. A.; Teimouri, A.; Chermahini, A. N.; Shahraki, M. *Spectrochim. Acta, Part A* **2008**, *69*, 449–459.
- (67) Varasanyi, G. *Assignments for Vibrational Spectra of Seven Hundred Benzene Derivatives*; Adam Hilger: London, 1974; Vols. 1–2.
- (68) Albayrak, Ç.; Kaştaş, G.; Odabaşoğlu, M.; Frank, R. *Spectrochim. Acta, Part A* **2011**, *81*, 72–78.
- (69) Usha Rani, A.; Sundaraganesan, N.; Kurt, M.; Cinar, M.; Karabacak, M. *Spectrochim. Acta, Part A* **2010**, *75*, 1523–1529.
- (70) Rastogi, K.; Palafox, M. A.; Tanwar, R. P.; Mittal, L. *Spectrochim. Acta, Part A* **2002**, *58*, 1989–1997.
- (71) Tanak, H.; Ağar, A.; Yavuz, M. *J. Mol. Model.* **2010**, *16*, 577–587.
- (72) Ünver, H.; Yıldız, M.; Özay, H.; Durlu, T. N. *Spectrochim. Acta, Part A* **2009**, *74*, 1095–1099.
- (73) Yıldız, M.; Kılıç, Z.; Hökelek, T. *J. Mol. Struct.* **1998**, *441*, 1–10.
- (74) Salman, S. R.; Kamounah, F. S. *Spectrosc. Lett.* **2002**, *35*, 327–335.
- (75) Alarcon, S. H.; Pagani, D.; Bacigalupo, J.; Olivieri, A. C. *J. Mol. Struct.* **1999**, *475*, 233–240.
- (76) Özbek, N.; Kavak, G.; Özcan, Y.; İde, S.; Karacan, N. *J. Mol. Struct.* **2009**, *919*, 154.
- (77) Pearson, R. G. *Proc. Natl. Acad. Sci. U.S.A.* **1986**, *83*, 8440–8841.
- (78) Okulik, N.; Jubert, A. H. *Internet Electron. J. Mol. Des.* **2005**, *4*, 17–30.

- (79) Politzer, P.; Laurence, P. R.; Jayasuriya, K.; McKinney, J. *Special issue of Environ. Health Perspect.* **1985**, *61*, 191–202.
- (80) Scrocco, E.; Tomasi, J. *Topics in Current Chemistry*; Springer Verlag: Berlin, 1973; Vol. 7, p 95.
- (81) Sun, Y. X.; Hao, Q. L.; Wei, W. X.; Yu, Z. X.; Lu, L. D.; Wang, X.; Wang, Y. S. *J. Mol. Struct. (THEOCHEM)* **2009**, *904*, 74–82.
- (82) Andraud, C.; Brotin, T.; Garcia, C.; Pelle, F.; Goldner, P.; Bigot, B.; Collet, A. *J. Am. Chem. Soc.* **1994**, *116*, 2094–2102.
- (83) Geskin, V. M.; Lambert, C.; Bredas, J. L. *J. Am. Chem. Soc.* **2003**, *125*, 15651–15658.
- (84) Nakano, M.; Fujita, H.; Takahata, M.; Yamaguchi, K. *J. Am. Chem. Soc.* **2002**, *124*, 9648–9655.
- (85) Sajan, D.; Joe, H.; Jayakumar, V. S.; Zaleski, J. *J. Mol. Struct.* **2006**, *785*, 43–53.
- (86) Zhang, R.; Du, B.; Sun, G.; Sun, Y. X. *Spectrochim. Acta, Part A* **2010**, *75*, 1115–1124.
- (87) Kleinman, D. A. *Phys. Rev.* **1962**, *126*, 1977–1979.
- (88) Thanthiriwatte, K. S.; Nalin de Silva, K. M. *J. Mol. Struct. (THEOCHEM)* **2002**, *617*, 169.
- (89) Maroulis, G.; Begue, D.; Pouchan, C. *J. Chem. Phys.* **2003**, *119*, 794.
- (90) Maroulis, G. *J. Chem. Phys.* **2008**, *129*, 044314.
- (91) Wu, K.; Snijders, J. G.; Lin, C. *J. Phys. Chem. B* **2002**, *106*, 8954–8958.
- (92) Li, D. Q.; Marks, T. J.; Ratner, M. A. *J. Phys. Chem.* **1992**, *96*, 4325–4336.
- (93) Ruiz Delgado, M. C.; Hernandez, V.; Casado, J.; Lopez Navarre, J. T.; Raimundo, J. M.; Blanchard, P.; Roncali, J. *J. Mol. Struct.* **2003**, *151*, 651–653.
- (94) Abraham, J. P.; Sajan, D.; Shettigar, V.; Dharmaprasanth, S. M.; Nemeč, I.; Hubert Joe, I.; Jayakumar, V. S. *J. Mol. Struct.* **2009**, *917*, 27–36.
- (95) Paine, S. W.; Salam, A. *Chem. Phys.* **2006**, *331*, 61–66.
- (96) Liu, L.; Guo, Q. X. *Chem. Rev.* **2001**, *101*, 673.
- (97) Hosseini, F. N. *Polyhedron* **2010**, *29*, 349.
- (98) Leung, D. H.; Bergman, R. G.; Raymond, K. N. *J. Am. Chem. Soc.* **2008**, *130*, 2798.
- (99) Starikov, E. B.; Norden, B. *J. Phys. Chem. B* **2007**, *111*, 14431.